

# Photon Emission from Dense Quark Matter

C. Vogt<sup>a 1</sup>, R. Rapp<sup>a,b 2</sup> and R. Ouyed<sup>c 3</sup>

<sup>a</sup>*Nordita, Blegdamsvej 17, 2100 Copenhagen, Denmark*

<sup>b</sup>*Cyclotron Institute and Physics Department, Texas A&M University, College Station, TX  
 77843-3366, USA*

<sup>c</sup>*Department of Physics and Astronomy, University of Calgary, 2500 University Drive NW,  
 Calgary, Alberta, T2N 1N4 Canada*

## Abstract

Thermal emission rates and mean free paths of photons in a color-flavor locked (CFL) phase of quark matter at high densities and moderate temperatures are evaluated. Our calculations are based on a low-energy effective theory for CFL matter describing Goldstone boson excitations and their electromagnetic as well as strong interactions. In-medium coupling strengths of vector mesons are estimated to be smaller than in vacuum. As a consequence of in-medium modified pion dispersion relations, novel processes such as  $\pi^+\pi^- \rightarrow \gamma$  and  $\gamma \rightarrow \pi^+\pi^-$  become possible. The total photon emissivity is found to be very large, exceeding contributions from thermal  $e^+e^-$  annihilation above temperatures of about 5 MeV. At the same time, the corresponding mean free paths become very small. Our results imply that the photon flux from the surface of a (hypothetical) CFL star in its early hot stages saturates the black-body limit. Schematic estimates for the early thermal evolution of the star are also presented.

## 1 Introduction

The discovery of asymptotic freedom, leading to the formulation of quantum chromodynamics (QCD) as the theory of strong interactions, was soon followed by the suggestion that matter at sufficiently high densities consists of a deconfined phase of quarks [1]. Only shortly afterwards it was pointed out [2] that the true ground state of cold dense quark matter exhibits color superconductivity (CSC), characterized by diquark condensation with an estimated energy gap  $\Delta$  of the order of 1 MeV between the highest occupied and the unperturbed quark state at the Fermi surface. Since this magnitude of the gap is rather small for phenomenological

---

<sup>1</sup>Email: cvogt@nordita.dk

<sup>2</sup>Email: rapp@comp.tamu.edu

<sup>3</sup>Email: ouyed@phas.ucalgary.ca

applications, CSC subsequently received little attention. The situation changed when reinvestigations [3, 4] using nonperturbative forces (*e.g.*, instanton-induced) showed that the gap can be substantially larger,  $\Delta \simeq 100$  MeV for moderate quark chemical potentials,  $\mu_q \simeq 350$  MeV. Similarly large values are obtained from estimates based on perturbative calculations at asymptotically high densities [5, 6]. Thus, from the practical point of view, the existence of color superconductivity in compact stars has (re-) emerged as an exciting possibility.

The detailed properties of CSC matter relevant to astrophysical applications depend on the interplay of the quark chemical potential, the  $q$ - $q$  interaction strength, and the bare masses of the (light) quarks  $u$ ,  $d$  and  $s$ . In particular, for  $\mu_q$  below the (constituent) strange quark mass, only  $u$  and  $d$  quarks are subject to BCS pairing. The corresponding phase is known as 2-flavor CSC (2SC). In the idealized case where the quark chemical potential is much larger than the strange quark mass ( $m_s$ ), the latter becomes negligible and all three flavors exhibit likewise pairing. The preferred symmetry (breaking) pattern in this phase corresponds to the so-called color-flavor locking (CFL) [7], since the underlying diquark condensate is invariant only under simultaneous color and flavor transformations. In the present work, we will focus on the CFL phase (for a recent review and a more exhaustive list of references, cf. [8]).

The investigation of compact stellar objects largely relies on electroweak emission spectra over a broad range of frequencies. Thus, emissivities and mean free paths ( $mfp$ 's) of neutrinos and photons are important quantities to assess bulk properties of matter within compact stars. It is therefore vital to address the question in how far the existence of CSC inside compact stars affects their properties, such as neutrino and photon emission as well as thermal evolution. Pertinent studies have recently been carried out for CSC phases in various scenarios [9, 10, 11]. Ref. [9] mostly addressed neutrino emission for CFL matter at temperatures in the sub-MeV range ( $\sim 0.1$  MeV or  $10^9$  Kelvin) relevant to the long-term evolution of a compact star. In Ref. [10] the CFL neutrino problem has been investigated for a temperature range of up to 30 MeV, corresponding to the hottest phases expected to occur during a supernova explosion or in the early stages of a proto-neutron star (see, *e.g.*, Ref. [12]). Photon emission has been calculated in Ref. [11] in a weak-coupling expansion for (gapped) quarks. The objective of the present article is to evaluate both photon emissivities and  $mfp$ 's in the strong coupling regime of CFL matter in the (tens of) MeV temperature region making use of an underlying effective theory description. The main processes of interest therefore involve scattering and decay processes of Goldstone bosons, taking into account their in-medium modified dispersion relations. For comparison, the effects of thermal electrons and positrons are assessed, which prevail towards lower temperatures. Furthermore, we incorporate generalized vector mesons, relevant at the high-temperature end of the CFL phase. As a lower limit, and in order to minimize the number of poorly known parameters, such as meson masses, we restrict the effective theory description to the  $SU(2)$  flavor sector, *i.e.*, neglect contributions from mesons involving strange quarks (cf. Ref. [13] for a recent analysis in hot hadronic matter). We will comment on the effects of kaons and other strangeness-bearing mesons in the summary.

The outline of the article is as follows. In Sect. 2 we will recall the basic elements of the effective low-energy Lagrangian which describes the electromagnetic and strong interactions of pseudoscalar Goldstone bosons. In Sect. 3 the evaluation of photon emission rates and mean free paths will be presented, including novel aspects specific to the CFL setting. Sect. 4 is devoted to an estimate of the photon-driven cooling behaviour in the early stages of the thermal evolution of a compact star which accommodates CFL matter throughout. Finally,

Sect. 5 contains our summary and conclusions. Explicit expressions for medium-modified Feynman rules and process amplitudes have been relegated to the Appendix.

## 2 Effective Low Energy Lagrangian

The effective low-energy theory of CFL diquark matter is analogous to the chiral theory in the QCD vacuum and has been introduced in Refs. [14, 15, 16]. Most notably, color-flavor locking induces the breaking of chiral and baryon number symmetries. Thus, an octet and singlet of pseudoscalar Goldstone bosons emerges which constitute the low-energy excitations and hence determine the features of CFL matter for energies below the gap, including electromagnetic and thermal properties. Although the (pseudo-) Goldstone bosons in CFL matter carry the same quantum numbers as in vacuum, differences in the chiral symmetry breaking pattern render their masses – arising from the explicit breaking due to finite current masses – qualitatively and quantitatively different. While in the vacuum case the parameters of the chiral Lagrangian have to be extracted from experiment, in the case of CFL matter a matching of the low-energy sector with the so-called high-density effective theory (HDET) allows for a determination of parameters in lowest order of the chiral and perturbative expansion, respectively. A detailed analysis for excitations below and above the gap revealed, *e.g.*, that the mass hierarchy in the strange and nonstrange sector is (partially) inverted [16, 17, 18].

The main objective of the present work is an assessment of electromagnetic and strong processes involving Goldstone-boson and vector excitations. As a convenient approach towards this goal, we here adopt the hidden local symmetry (HLS) framework that, in the context of CFL matter, was suggested in Ref. [19] and further elaborated in Ref. [11]. It amounts to a treatment of vector mesons as dynamical, composite gauge bosons corresponding to a hidden local  $SU(3)_{c+L+R}$  symmetry.<sup>4</sup> Originally, the HLS approach was introduced in the vacuum case in Ref. [20] (for a review see [21]). Here, we will briefly recall the main elements important for our work.

We start with the effective chiral Lagrangian of (generalized) pseudoscalar Goldstone bosons in the CFL phase, which is equivalent to the non-linear sigma model known from the vacuum and reads [14, 15, 16]

$$\mathcal{L}_{\text{eff}} = \frac{f_\pi^2}{4} \text{Tr} [\partial_0 U \partial_0 U^\dagger - v_\pi^2 \partial_i U \partial_i U^\dagger] - c [\det(M) \text{Tr} (M^{-1} U) + h.c.] , \quad (1)$$

with  $M = \text{diag}(m_u, m_d, m_s)$  being the current quark mass matrix. The chiral field  $U$  is related to the Goldstone boson octet  $\pi \equiv \pi^a \lambda^a$  by

$$U = e^{i\pi/f_\pi} , \quad (2)$$

where the Gell-Mann flavor matrices are normalized as  $\text{Tr}[\lambda^a, \lambda^b] = 2\delta^{ab}$  and  $f_\pi$  is the (in-medium) pion decay constant. The latter, as well as the constant  $c$  in Eq. (1), can be obtained from the matching procedure, referred to above, to leading order in  $\alpha_s$  [16],

$$f_\pi^2 = \frac{21 - 8 \ln 2}{18} \frac{\mu_q^2}{2\pi^2} , \quad c = \frac{3\Delta^2}{2\pi^2} . \quad (3)$$

---

<sup>4</sup>Strictly speaking, hidden local symmetry only holds in the zero size approximation, neglecting the finite size of condensed diquarks, cf. Ref. [19] for a discussion of this issue.

The explicit expressions for the pion masses then take the form [18]

$$m_{\pi^\pm} = \mp \frac{m_d^2 - m_u^2}{2\mu_q} + \left[ \frac{3\Delta^2}{\pi^2 f_\pi^2} (m_u + m_d) m_s \right]^{1/2}. \quad (4)$$

As Lorentz invariance is broken due to the rest frame of the medium, the pion decay constant (defined via the weak pion decay matrix element) generally splits into temporal and spatial components [22], denoted by  $f_T$  and  $f_S$ , respectively. They are related to the pion velocity  $v_\pi$  (found to be  $v_\pi = 1/\sqrt{3}$ , coinciding with the speed of sound in relativistic fluids [16]) through  $f_S = v_\pi^2 f_T$ , with  $f_T = f_\pi$ . Consequently, the pion velocity also appears in the effective Lagrangian (1), and induces a modified dispersion relation for the Goldstone bosons, which follows from the corresponding kinetic term as

$$E = \sqrt{m_{\text{GB}}^2 + v_\pi^2 \mathbf{p}^2}. \quad (5)$$

The hidden local symmetry of the low-energy effective theory, Eq. (1), can be made explicit by decomposing the left and right pion fields  $\pi_{L,R}$  according to

$$U_{L,R} = e^{i\pi_{L,R}/f_\pi} = \xi_c^T \xi_{L,R}, \quad (6)$$

where  $\xi_c$  and  $\xi_{L,R}$  are  $SU(3)$  color and chiral gauge fields, respectively. In the following, we will fix the local  $SU(3)_{c+L+R}$  gauge by  $\xi_c = \xi_{L,R} \equiv \xi$ , which identifies the left and right pion fields and reflects the color-flavor locking property. In terms of the field  $\xi$ , the kinetic term of the Lagrangian (1) then reads

$$\mathcal{L}_{\text{kin}} = -\frac{f_\pi^2}{4} \text{Tr} \left[ \partial_0 \xi \xi^\dagger - \xi \partial_0 \xi^\dagger + v_\pi^2 (\partial_i \xi \xi^\dagger - \xi \partial_i \xi^\dagger) \right]^2. \quad (7)$$

We proceed by introducing both the vector field,  $V_\mu = V_\mu^a \lambda^a/2$ , and the in-medium photon field,  $\tilde{A}_\mu$ , by means of the covariant derivative [20]

$$D_\mu \xi = \partial_\mu \xi - i\tilde{g} V_\mu \xi - i\tilde{e} \xi \tilde{A}_\mu Q, \quad (8)$$

with  $Q = \text{diag}(2/3, -1/3, -1/3)$  being the quark-charge matrix. The vector-meson field is rendered dynamical in the usual manner by introducing a kinetic term  $-(1/4) \text{Tr} F_{\mu\nu} F^{\mu\nu}$ , where  $F_{\mu\nu} = \partial_\mu V_\nu - \partial_\nu V_\mu + i\tilde{g} [V_\mu, V_\nu]$  is the field strength tensor.

As noted in Ref. [7], the electromagnetic coupling in the CFL phase is modified. Since a diquark condensate carries baryon number, the physical (massless) photon field in medium is a linear combination of the original photon and the eighth component of the gluon field. The electric charge  $\tilde{e}$  in medium is therefore related to the vacuum charge  $e$  and strong coupling  $g_s$  via  $\tilde{e} = e \cos \theta$  where  $\cos \theta = \sqrt{3} g_s / \sqrt{3g_s^2 + 4e^2}$ . Since, over a wide range of momenta, the strong coupling is much larger than the electromagnetic one, we will, for practical purposes, set  $\cos \theta \simeq 1$  and drop the tilde notation for the photon field and the electromagnetic coupling in the following. The introduction of the electroweak interaction in the effective Lagrangian of the CFL and 2SC phases is presented in detail in Ref. [23].

The question now arises how to determine the masses and coupling strengths of the vector mesons in the CFL environment. In Ref. [11], where the HLS approach has first been

adopted to evaluate dilepton emission rates from CFL matter, vector-meson dominance (VMD) was assumed in connection with  $\tilde{g} = g_{\rho\pi\pi}$  at its vacuum value ( $\sim 6$ ). From the KSFR relation [24] it was then inferred that the vector-meson mass scales with the chemical potential  $\mu_q$ . On the other hand, in Ref. [19] a detailed weak-coupling calculation based on a Bethe-Salpeter equation has identified the axial/vector excitations (mesons) as diquark-hole states resulting in

$$m_V = 2 \Delta \sqrt{1 - e^{-C/\tilde{g}}} , \quad (9)$$

which for all practical purposes equals twice the gap ( $C = (3 - \sqrt{3}) \pi^2 \sqrt{6} \simeq 30.7$ ). In the recent work of Ref. [25], the (parametric) dependence of Eq.(9),  $m_V \propto \Delta$ , was corroborated by a nonperturbative argument, *i.e.*, by matching higher-derivative contact terms of the low-energy effective theory, Eq. (1), with local terms obtained as a result of integrating out the heavy  $V$ -fields in a generic chiral Lagrangian. Thus, we henceforth adopt  $m_V = 2 \Delta$  also for the present case of a strong coupling environment, and do not distinguish between temporal and spatial vector-meson masses  $m_T$  and  $m_S$  as was done in Ref. [11]. The vector-meson mass term in the Lagrangian then acquires the standard vacuum form  $(m_V^2/2) V_\mu V^\mu$ .

Within the matching procedure of Ref. [25] it has furthermore been found that the vector-coupling strength scales according to<sup>5</sup>

$$\tilde{g} \propto \frac{\Delta}{f_\pi} . \quad (10)$$

This result suggests that, for large chemical potential, the self-interactions of the vector mesons are reduced with respect to (*w.r.t.*) the vacuum. By expanding the effective Lagrangian in the Goldstone boson fields, we see that  $\tilde{g}$  is identical to the coupling strength  $g_{\rho\pi\pi}$  of the vector meson to two pions. In particular,  $g_{\rho\pi\pi}$  scales in the same way as  $\tilde{g}$ . While in vacuum  $g_{\rho\pi\pi} = \tilde{g} \simeq 6$ , the corresponding values in the CFL phase are parametrically suppressed. To obtain a more quantitative estimate for the  $\rho\pi\pi$  coupling, we follow Refs. [11, 25] in assuming that the KSFR relations remain valid in CFL matter, *i.e.*,

$$m_V^2 = 2 \tilde{g}^2 f_\pi^2 . \quad (11)$$

Here we have also assumed that VMD remains intact, implying that the HLS parameter has been fixed at  $a = 2$ .<sup>6</sup> For the vector-meson interaction strength and their coupling to the Goldstone bosons we then have<sup>7</sup>

$$g_{\rho\pi\pi} = \tilde{g} \simeq \sqrt{2} \frac{\Delta}{f_\pi} . \quad (12)$$

---

<sup>5</sup>Using duality arguments, the analysis in [25] also exhibits that nucleon-type excitations are parametrically heavy with their masses proportional to  $f_\pi^2/\Delta$ . However, at moderate densities, where  $f_\pi$  is not larger than the gap, this assertion no longer holds, and the (solitonic) “nucleon” or “delta” masses could become comparable to the vector meson ones; for large pairing gaps, it would thus be interesting to evaluate the effects of  $\pi$ - $N$  interactions – known to be strong in ordinary hadronic matter – in a CFL environment at temperatures above 10 MeV.

<sup>6</sup>In the weak-coupling analysis of Ref. [26] it was found that the KSFR relations are modified at asymptotic densities, resulting in  $a=1$ . A similar feature arises within a renormalization-group treatment of the HLS approach at the finite temperature chiral phase transition [27].

<sup>7</sup>We would like to thank F. Sannino for pointing this out to us.

With a typical parameter choice of  $\Delta_0 = 50 - 150$  MeV at  $\mu_q \simeq 350$  MeV (the latter implying  $f_\pi \simeq 73$  MeV), one obtains  $g_{\rho\pi\pi} \simeq 1 - 2.8$ , substantially smaller than in free space.

For the reasons discussed above, we employ the vacuum form of the vector-meson mass term, implying that the vector-meson propagator is identical to the vacuum propagator. In order to preserve gauge invariance, it then turns out that also VMD needs to be applied in its vacuum version, *i.e.*, without the distinction of temporal and spatial components in the  $V$ - $\gamma$  vertex. Technically, this amounts to introducing into the Lagrangian a counter term of the form

$$4 e \tilde{g} f_\pi^2 \text{Tr} (A_0 Q V_0 - v_\pi^2 A_i Q V_i) - \frac{2 m_V^2}{\tilde{g}} e A_\mu \text{Tr} (Q V^\mu) , \quad (13)$$

where the last term represents the standard  $V$ - $\gamma$  vertex<sup>8</sup>. Thus, after substituting the covariant derivative (8) in expression (7) and expanding in the pion field  $\pi$ , the complete interaction part of our Lagrangian for Goldstone bosons now reads

$$\begin{aligned} \mathcal{L}_{\text{GB,int}} = & -i \frac{g_{\rho\pi\pi}}{2} \text{Tr} \left( V_0 [\pi, \partial_0 \pi] + v_\pi^2 V_i [\pi, \partial_i \pi] \right) + \frac{e^2}{4} (A_0^2 - v_\pi^2 A_i^2) \text{Tr} ([Q, \pi])^2 \\ & - \frac{e g_{\rho\pi\pi}}{2} \text{Tr} \left( A_0 [V_0, \pi] [Q, \pi] - v_\pi^2 A_i [V_i, \pi] [Q, \pi] \right) - \frac{2 m_V^2}{\tilde{g}} e A_\mu \text{Tr} (Q V^\mu) . \end{aligned} \quad (14)$$

VMD reflects itself by the absence of a direct  $\pi\pi\gamma$  interaction term. Finally, the physical photon and vector-meson field can be obtained by the usual diagonalization procedure. Note that, within the present approach, all parameters of the low-energy effective Lagrangian are now fixed.

### 3 Photon Emission and Absorption

Let us turn to the evaluation of the photon emission rates and mean free paths in CFL matter as a function of temperature and the value of the zero-temperature gap. As mentioned in the introduction, we restrict ourselves to processes within the  $SU(2)$  flavor sector, *i.e.*, charged and neutral pions, as well as rho mesons. Since at temperatures of  $\mathcal{O}(1 \text{ MeV})$ ,  $e^+e^-$  pairs have comparatively large number densities [10], they will also be included in our analysis. For definiteness, we assume the validity of the BCS relation for the gap,  $\Delta = \Delta_0 \sqrt{1 - (T/T_c)^2}$ , with a critical temperature  $T_c \simeq 0.56 \Delta_0$ . In order to demonstrate the dependence of our results on the (poorly known) gap, we perform our calculation with two different values,  $\Delta_0 = 50$  MeV and  $\Delta_0 = 150$  MeV. Unless otherwise stated, we set  $\mu_q = 350$  MeV.

#### 3.1 Emission Rates and Emissivities

The general set-up for the calculation of photon emission rates follows the ones performed in an ordinary hot meson gas in Refs. [28, 29]. The obvious differences expected in a CFL phase are due to the different masses and strong couplings of the pions and rho mesons, as

---

<sup>8</sup>A similar procedure of restoring gauge invariance is often adopted when, *e.g.*, including vertex form factors in hadronic effective theories [28]. The underlying microscopic origin of the counter terms remains open.

well as the modified pion dispersion relation. Both of these features lead to an increase in available phase space. The CFL pions are considerably lighter than in vacuum. Fixing the current quark masses at  $m_u = 3$  MeV,  $m_d = 7$  MeV and  $m_s = 120$  MeV, we find  $m_\pi \simeq 12$  (38) MeV for  $\Delta_0 = 50$  (150) MeV and temperatures of  $\mathcal{O}(10)$  MeV. Throughout our numerical calculations, the temperature dependence of the pion mass, entering through  $\Delta(T)$  in Eq. (4), will be accounted for.

The relevant processes which lead to one or two photons in the final state, are scattering of the form  $M_1 M_2 \rightarrow M_3 \gamma$  (where  $M_i$  are pseudoscalar or vector mesons), annihilation,  $M_1 M_2 \rightarrow \gamma \gamma$ , and rho-meson decays,  $\rho \rightarrow \pi \pi \gamma$ . The (anomalous) neutral pion decay,  $\pi^0 \rightarrow \gamma \gamma$ , has been considered in Ref. [9] for low temperatures of  $\mathcal{O}(0.1)$  MeV, where the emissivity was found to be exponentially suppressed. For completeness, we have repeated the calculation for the larger temperatures we are interested in here. Note that purely electromagnetic processes, *e.g.*,  $\pi^+ \pi^- \rightarrow \gamma \gamma$ , are relatively suppressed by a factor  $e^2/g_{\rho\pi\pi}^2 \simeq 10 - 100$  as compared to strong processes such as  $\pi^+ \pi^- \rightarrow \rho^0 \gamma$ . At low temperatures, however, strong processes, requiring at least one in- or outgoing rho meson, are penalized by thermal suppression due to the relatively large rho mass. The in-medium Feynman rules and explicit expressions for the amplitudes are summarized in Appendix A.1 and A.2, respectively. We have verified that all amplitudes satisfy electromagnetic gauge invariance.

In addition to the above processes, which can all occur in a vacuum environment, a novel photon source arises due to the medium-modified pion dispersion relation. With the in-medium pion velocity  $v_\pi < 1$ , annihilation of the type  $\pi^+ \pi^- \rightarrow \gamma$  can become kinematically allowed, *i.e.*, with all particles being *on-mass shell*. This is rendered possible due to the pion invariant-mass,  $p^2 = m_\pi^2 - (1 - v_\pi^2) \mathbf{p}^2$ , being reduced and eventually turning spacelike at large 3-momentum. Thus, sufficiently fast pions can annihilate on slow ones. A more detailed discussion of this effect, which also proceeds in the inverse direction, thereby contributing to photon absorption, will be given in Sect. 3.3.

The photon emission rate for a given process, *e.g.*,  $M_1(p_1) M_2(p_2) \rightarrow M_3(p_3) \gamma(q)$ , is obtained from a phase space integral over the pertinent unpolarised scattering amplitude,  $\mathcal{M}$ , according to

$$E \frac{dR}{d^3q} = \frac{\mathcal{N}}{2(2\pi)^3} \int \frac{d^3\mathbf{p}_1}{(2\pi)^3 2E_1} \int \frac{d^3\mathbf{p}_2}{(2\pi)^3 2E_2} \int \frac{d^3\mathbf{p}_3}{(2\pi)^3 2E_3} (2\pi)^4 \delta^{(4)}(p_1 + p_2 - p_3 - q) \\ \times \left| \mathcal{M}^{M_1 M_2 \rightarrow M_3 \gamma} \right|^2 f(E_1, T) f(E_2, T) [1 + f(E_3, T)], \quad (15)$$

where  $\mathcal{N}$  is a (spin-isospin) degeneracy factor and  $f(E_i, T)$  are Bose-Einstein distribution functions. To evaluate the integral, we rewrite

$$\int \frac{d^3\mathbf{p}_i}{(2\pi)^3 2E_i} = \int \frac{d^4p_i}{(2\pi)^3} \delta(E_i^2 - m_i^2 - v_i^2 \mathbf{p}_i^2) \Theta(E_i), \quad (16)$$

with  $v_i$  being the velocity of particle  $i$  (different from 1 only for Goldstone bosons in the present work). One can then perform one of the 4-dimensional phase space integrations (for definiteness,  $i = 3$ ) exploiting the  $\delta$ -function in Eq. (15). Since rotational symmetry persists in the medium, we may fix the photon momentum  $\mathbf{q}$  in  $z$ -direction for subsequent purposes. The remaining angular dependences consist of the cosine of the polar angles,  $\cos \theta_1$  and  $\cos \theta_2$ , of particles 1 and 2 (*w.r.t.* the  $z$ -axis), and their relative azimuth  $\phi = \phi_1 - \phi_2$  (the integration

over the total azimuth  $\Phi = \phi_1 + \phi_2$  becomes trivial). With  $d^3p_j = |\mathbf{p}_j|^2 d|\mathbf{p}_j| d\Omega_j$  and  $E_j dE_j = v_j^2 |\mathbf{p}_j| d|\mathbf{p}_j|$  for  $j=1, 2$ , we arrive at

$$\begin{aligned} E \frac{dR}{d^3q} &= \frac{2\pi \mathcal{N}}{8(2\pi)^8} \int \frac{|\mathbf{p}_1| dE_1 d\cos\theta_1}{v_1^2} \int \frac{|\mathbf{p}_2| dE_2 d\cos\theta_2}{v_2^2} d\phi \Theta(E_1 + E_2 - E) \\ &\quad \times \delta\left((E_1 + E_2 - E)^2 - m_i^2 - v_i^2 (\mathbf{p}_1 + \mathbf{p}_2 - \mathbf{q})^2\right) \left| \mathcal{M}^{M_1 M_2 \rightarrow M_3 \gamma} \right|_{p_3=p_1+p_2-q}^2 \\ &\quad \times f(E_1, T) f(E_2, T) [1 + f(E_1 + E_2 - E, T)]. \end{aligned} \quad (17)$$

For external (on-shell) particles, the energy integrations are restricted from below by  $E_{i,\min} = m_i$ . The  $\phi$  integration can be performed using the remaining  $\delta$ -function at its zero argument,  $\phi_0$ , generating a Jacobian factor  $[2 v_i^2 |\mathbf{p}_1| |\mathbf{p}_2| |\sin\theta_1 \sin\theta_2 \sin\phi_0|]^{-1}$ . The last four integrations are carried out numerically.

The results for the emission rates in CFL matter for different gap values and temperatures are summarized in Fig. 1. As a check of our numerical calculation, we have ensured agreement with the results of Refs. [28, 29] when using the vacuum values for masses (and velocities) of the pseudoscalar and vector mesons (pertinent curves for  $T = 50$  MeV are displayed in the lower right panel of Fig. 1). Comparing the lower two panels, one observes that photon emission from CFL matter is strongly enhanced, which is essentially due to the increased phase space, as mentioned above. The particularly large rates for the processes  $\pi^+\pi^- \rightarrow \gamma\gamma$  and  $\pi\rho \rightarrow \pi\gamma$  have their origin in the modified pion dispersion relation to be discussed in Sec. 3.3. The upper two panels indicate that strong processes involving rho mesons are further enhanced for smaller gap values, due to the reduced rho-meson mass. The emission rate for  $\pi^0 \rightarrow \gamma\gamma$  is only shown in the vacuum case. In CFL matter this rate is kinematically suppressed: it vanishes if the photon energy is larger than  $m_\pi/\sqrt{1-v_\pi^2}$ . We finally remark that finite size effects of the effective meson states, *i.e.*, vertex form factors, have not been included here (for a recent assessment of their suppression effects in photon production at high energies in normal hot hadronic matter, cf. Ref. [13]).

The total photon emissivities, *i.e.*, the emitted photon energies per unit volume and time, are now easily obtained by integrating the emission rate (15) (multiplied by the corresponding Bose enhancement factor) over the photon 3-momentum,

$$\epsilon_\gamma = \int d^3q \left( E \frac{dR}{d^3q} \right) [1 + f(E, T)]. \quad (18)$$

Note that due to rotational symmetry the angular integration in the variable  $\mathbf{q}$  can be done trivially yielding a factor  $4\pi$ . The photon emissivity for all processes in CFL matter presently investigated is shown in Fig. 2. The process  $e^+e^- \rightarrow \gamma\gamma$  dominates up to temperatures of about 3 (7) MeV for  $\Delta_0 = 50$  (150) MeV. For larger  $T$ ,  $\pi^+\pi^- \rightarrow \gamma\gamma$  prevails. Strong processes involving rho mesons start to compete at temperatures of about 20 (25) MeV for  $\Delta_0 = 50$  (150) MeV. However, the rho contributions are rather sensitive to the value of the rho-mass, subject to appreciable uncertainties due to, *e.g.*, (i) sizable corrections to the leading-log estimate, Eq. (9), (ii) finite width effects (not included at present) from the  $\rho \leftrightarrow \pi\pi$  coupling, which extend the  $\rho$  spectral strength down to the two-pion threshold. Therefore, our current calculations cannot yet reliably determine at which temperatures strong processes outshine the electromagnetic ones. Finally, let us point out that, due to the (partial) inversion of the mass



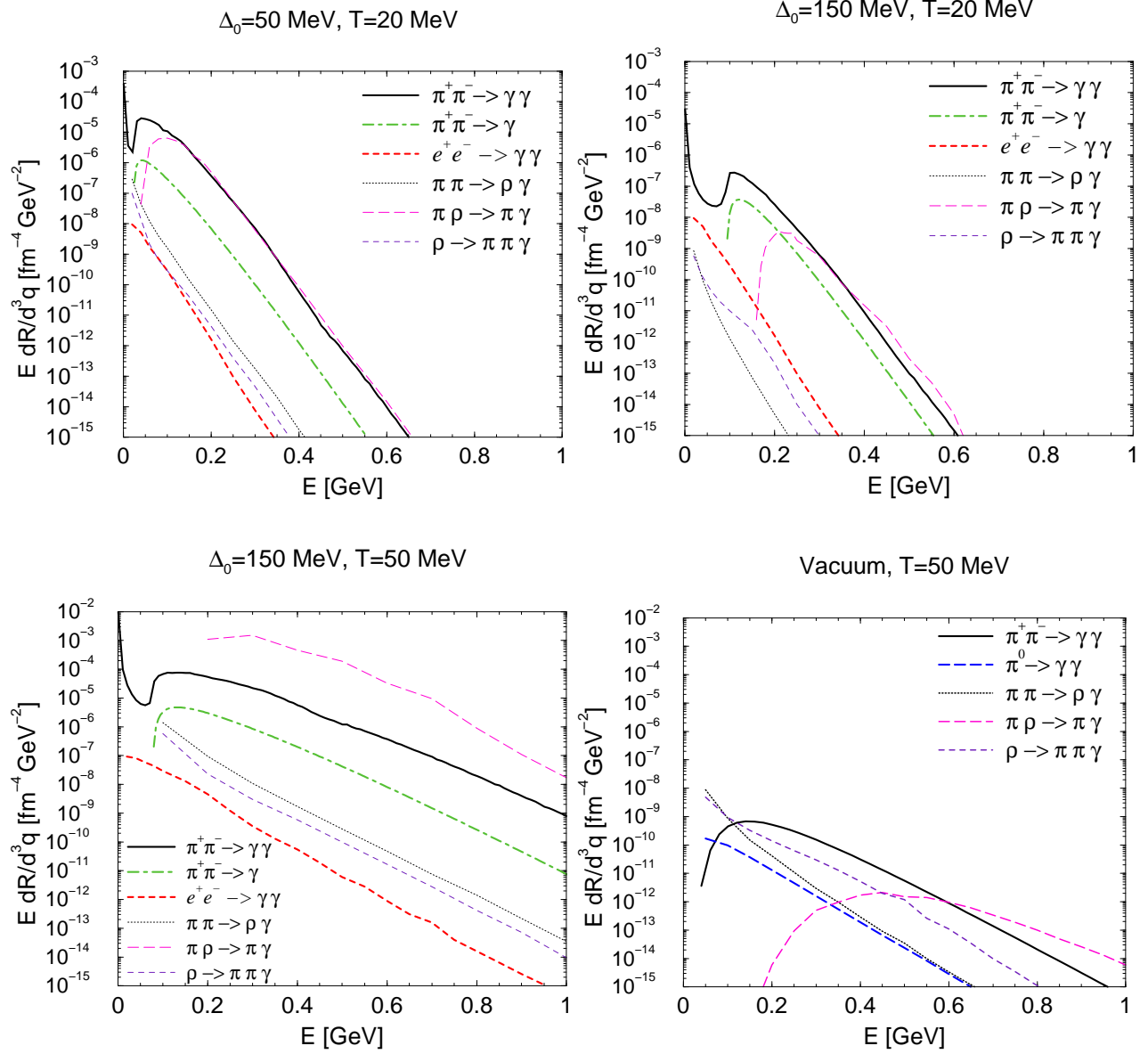


Figure 1: Photon emission rates in CFL matter from various electromagnetic (thick lines) and strong-interaction (thin lines) sources as a function of the photon energy  $E$ . Upper plots:  $\Delta_0 = 50$  MeV (left) and  $\Delta_0 = 150$  MeV (right) at  $T = 20$  MeV; lower plots:  $\Delta_0 = 150$  MeV (left) and vacuum phase (right) at  $T = 50$  MeV.

hierarchy in the strange and nonstrange sector referred to in Sect. 2.1, we expect contributions from kaon pairs to be important or even dominant. These are not included at present, but can be treated by a straightforward extension of our calculations to  $SU(3)_F$ .

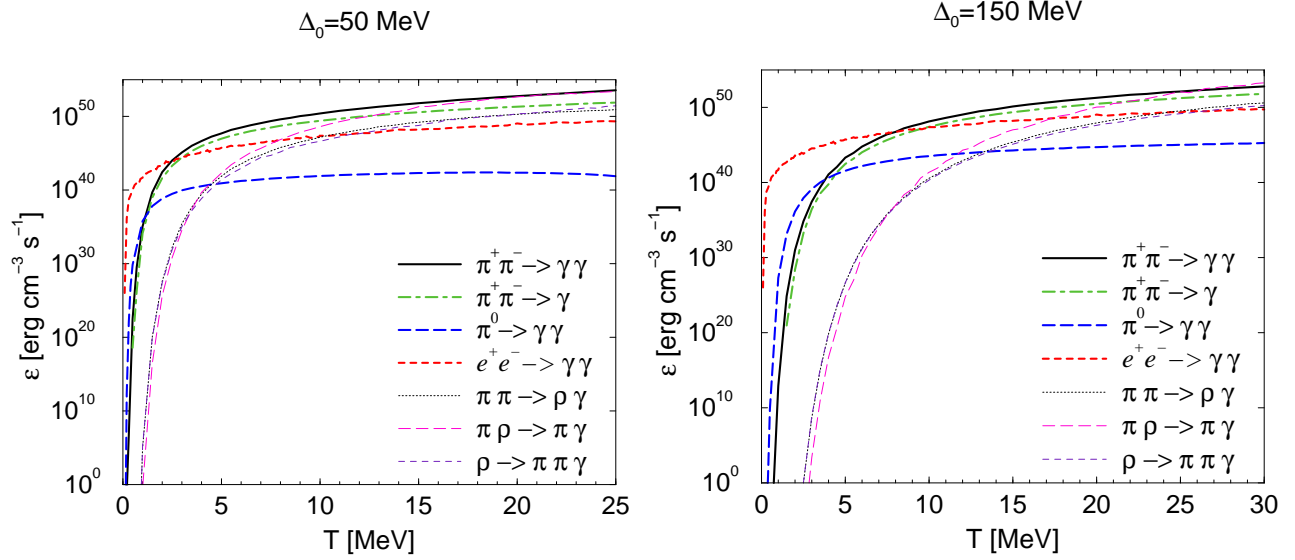


Figure 2: Photon emissivities in CFL matter from various electromagnetic (thick lines) and strong-interaction (thin lines) sources as a function of the temperature for  $\Delta_0 = 50$  MeV (left) and  $\Delta_0 = 150$  MeV (right).

### 3.2 Mean free path

To estimate the emitted photon luminosity of a finite size object an assessment of the pertinent mean free path is mandatory. In CFL matter, the latter is governed by Compton scattering off the light charged excitations, as well as photon annihilation reactions. In the  $SU(2)$  flavor sector, the lightest charged excitations are the pions as well as electrons and positrons. Similar to the emissivity discussed in the previous Section, at low  $T \sim 1$  MeV one can expect processes involving  $e^\pm$  to be dominant (due to their relatively large number densities), whereas towards higher  $T$  reactions involving pions ought to take over. As mentioned in the preceding subsection, another contribution arises from the novel “decay” process  $\gamma \rightarrow \pi^+\pi^-$ , which owes its existence to the in-medium modified pion dispersion relation.

The inverse  $mfp$  of a photon of energy  $E$  is given by its total cross section on all medium particles per unit volume (schematically  $\langle \sigma_{\gamma X} n_X \rangle$  for each particle species  $X$  of density  $n_X$ ). For Compton scattering,  $\gamma(q) X^\pm(p_1) \rightarrow \gamma(q') X^\pm(p_2)$ , one has

$$\begin{aligned} \frac{1}{\lambda(E)} &= \frac{1}{2E} \int \frac{d^3\mathbf{p}_1}{(2\pi)^3 2E_1} \int \frac{d^3\mathbf{p}_2}{(2\pi)^3 2E_2} \int \frac{d^3\mathbf{q}'}{(2\pi)^3 2E'} (2\pi)^4 \delta^{(4)}(q + p_1 - q' - p_2) \\ &\quad \times \left| \mathcal{M}^{\gamma X^\pm \rightarrow \gamma X^\pm} \right|^2 f(E_1, T) [1 \pm f(E_2, T)] [1 + f(E', T)], \end{aligned} \quad (19)$$

where the upper (lower) sign holds for  $X=\pi$  ( $e$ ) in connection with Bose-Einstein (Fermi-Dirac) distributions  $f(E_1, T)$  and  $f(E_2, T)$ . Here, the process amplitude  $\mathcal{M}$  is averaged over the initial photon polarisation and summed over all others. An analogous expression holds for  $\gamma\gamma \rightarrow e^+e^-$  annihilation.

In Fig. 3 we display our results for the  $mfp$  at a typical thermal energy of the incoming photon,  $E = 3T$ . We confirm that for  $\Delta_0 = 50$  (150) MeV Compton scattering off  $e^\pm$  prevails

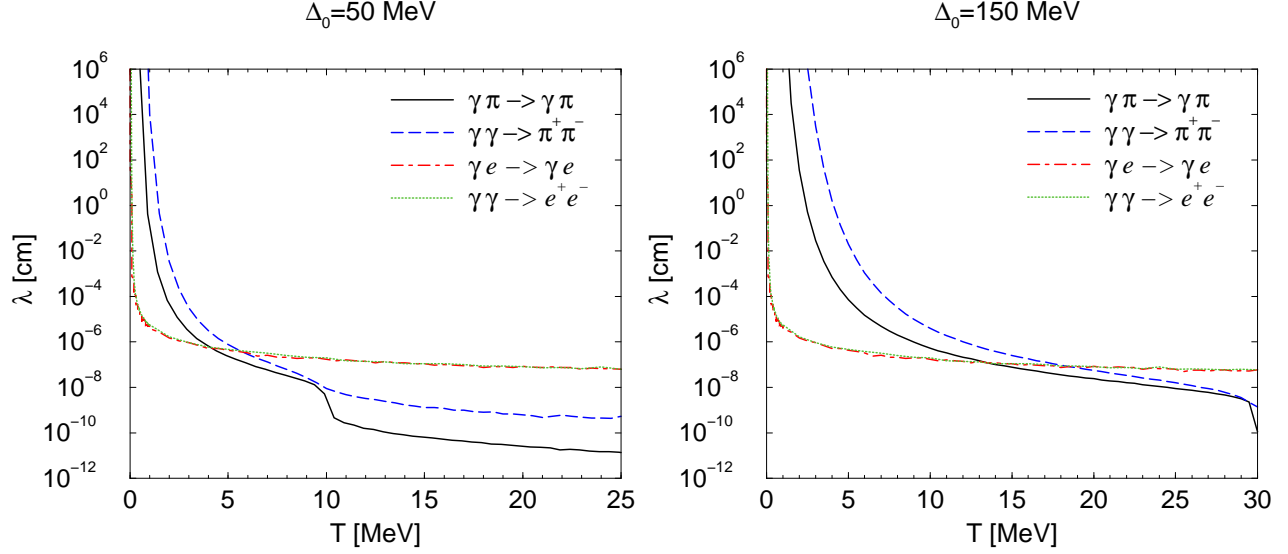


Figure 3: Photon mean free path from Compton scattering off  $\pi^\pm$ ,  $e^\pm$ , and photon annihilation into  $e^\pm$  and  $\pi^\pm$  pairs, for  $\Delta_0 = 50$  MeV (left) and  $\Delta_0 = 150$  MeV (right).

for temperatures of up to about 5 (15) MeV, while at larger temperatures, charged pions are the more relevant scatterers. Photon “decay” into two pions can only occur if the photon energy  $E \geq 2m_\pi/(1 - v_\pi^2)$ , which for  $E = 3T$  implies a minimum temperature  $T_{\min} = m_\pi$ . Hence, this novel process does not play a significant role at low temperatures. As we will elaborate in the following Section, it becomes however relevant for  $T \geq m_\pi$ . This induces the rather sharp decrease of the solid line in Fig. 3 around  $T \simeq 10$  MeV (left) and  $T \simeq 30$  MeV (right), corresponding to the pion mass for  $\Delta_0 = 50$  MeV and  $\Delta_0 = 150$  MeV, respectively.

### 3.3 In-Medium Pion Dispersion Effects

We now return to the specific effects of the in-medium pion velocity which are at the origin of the novel emission and absorption processes,  $\pi^+\pi^- \rightarrow \gamma$  and  $\gamma \rightarrow \pi^+\pi^-$ , respectively, already mentioned above. To illustrate their appearance in our calculations, let us for definiteness consider the reaction  $\pi^+\rho^0 \rightarrow \pi^+\gamma$ . This process has a contribution from a  $t$ -channel pion-exchange diagram. According to Eq. (29), the pertinent propagator,  $D_\pi$ , is modified by a factor  $v_\pi^2$  in the denominator, so that it takes the explicit form

$$D_\pi^{-1}(p_0, \mathbf{p}) = p_0^2 - v_\pi^2 \mathbf{p}^2 - m_\pi^2 = E^2(1 - v_\pi^2) - 2E(E_1 - v_\pi \sqrt{E_1^2 - m_\pi^2} \cos \Theta_1). \quad (20)$$

As before,  $E$  is the final-state photon energy,  $E_1$  the initial-state pion energy,  $\Theta_1$  the polar angle between their three momenta (the  $z$ -axis is chosen along the direction of the photon momentum), and  $t = p^2 = (p_1 - q)^2$  is the four-momentum of the exchanged *positively* charged pion. In vacuum ( $v_\pi = 1$ ),  $D_\pi^{-1}$  is always negative, *i.e.*, in the spacelike regime. In the medium, however, the presence of the term  $E^2(1 - v_\pi^2)$  implies that  $D_\pi^{-1}$  can become timelike and therefore develop singularities in the physical region. Evidently, timelike values can only occur for sufficiently large photon energies. If, *e.g.*, the incoming pion is at rest,  $D_\pi^{-1} = 0$

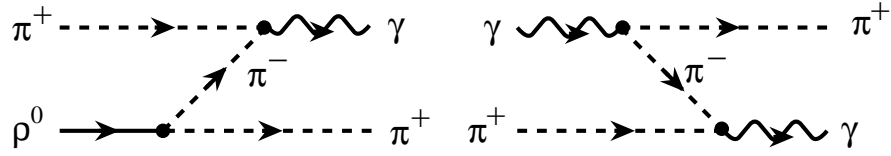


Figure 4: Z-graph contribution to  $\pi^+ \rho^0 \rightarrow \pi^+ \gamma$  and  $\gamma \pi^+ \rightarrow \gamma \pi^+$ . In time-ordered perturbation theory these diagrams have a cut with three pion states. Arrows are pointing in the direction of momentum flow.

requires a minimal photon energy of  $E_{\min} = 2m_\pi/(1 - v_\pi^2)$ . Furthermore, in this situation the intermediate pion carries negative energy, readily interpreted as being its antiparticle with positive energy and reversed three momentum, that is, an *incoming, on-mass-shell*,  $\pi^-$ . In the language of time-ordered perturbation theory this process represents a *Z-graph* contribution, depicted in the left panel of Fig. 4, where the incoming  $\pi^+$  annihilates with an intermediate  $\pi^-$  to produce the outgoing photon. The final scattering off the incoming  $\rho^0$  to bring the  $\pi^+$  on-shell is no longer required, contrary to the vacuum case. In vacuum, the virtual  $\pi^+$  only goes on-mass shell in the limit of zero photon energy, in which case the phase space vanishes, and the emissivity receives no contribution. Completely analogous arguments apply for other charge combinations of the process  $\pi \rho \rightarrow \pi \gamma$ .

One can verify the above features more explicitly by directly analyzing the process  $\pi(p_1) + \pi(p_2) \rightarrow \gamma(q)$ . Exploiting both energy and momentum conservation,  $E_1 + E_2 = E$  and  $\mathbf{p}_1 + \mathbf{p}_2 = \mathbf{q}$ , together with the on-mass shell dispersion relations for all three particles involved, one finds for  $\cos \Theta_1 = \pm 1$ :

$$E^\pm = 3E_1 \pm |\mathbf{p}_1|, \quad (21)$$

where we have used that  $v_\pi^2 = 1/3$ . This, in particular, implies that for an outgoing photon its (positive) energy  $E$  is always larger than  $E_1$  and therefore  $E_2 > 0$ , that is, the Bremsstrahlungs-process  $\pi(p_1) \rightarrow \pi(p_2) \gamma(q)$  is not possible.<sup>9</sup>

A similar discussion of the in-medium pion dispersion effects pertains to processes that contribute to the mean free path. As we have already pointed out in the previous Section, at a temperature corresponding to the pion mass the pion-induced mean free path exhibits a rather sharp decrease. In our calculation this is associated with the *u*-channel diagram in  $\gamma \pi$  Compton scattering, which exhibits a behaviour analogous to the *t*-channel diagram discussed above, *i.e.*, the intermediate pion becomes on-shell with negative energy. The interpretation via the corresponding Z-graph is that the incoming photon spontaneously decays into two on-shell charged pions, cf. the right panel of Fig. 4.

For the numerical evaluation of the diagrams involving on-shell intermediate pions we include in the (singular) pion-exchange propagators a finite width that can be attributed, *e.g.*, to interactions with surrounding medium pions. A schematic estimate of the pion width is given in Appendix A.3. For the present purpose it is sufficient to approximate the width by a constant; in the kinematical range of interest the evaluation of  $\rho \pi \pi$  interactions yields as an upper estimate a value of  $\Gamma_\pi \simeq 0.1$  MeV for  $\Delta_0 = 50$  MeV and  $\Gamma_\pi \simeq 0.01$  MeV for  $\Delta_0 = 150$  MeV.

<sup>9</sup>Equivalently, one can start from energy and momentum conservation for the Bremsstrahlungs-diagram to find that  $E_2$  must be negative, which again means that only the annihilation process can occur.

### 3.4 Comparison with Neutrino Properties

At this point, a comparison with the results of Ref. [10] is in order, where an analogous investigation of neutrino emissivities and mean free paths was presented. On the one hand, we find that the photon emissivity exceeds the neutrino emissivity by more than ten orders of magnitude over the entire temperature region. On the other hand, as to be expected for weakly interacting neutrinos, their mean free path is larger than that of photons by several orders of magnitude.

To confront the efficiencies of photon and neutrino emission in the radiation of energy from a hypothetical CFL star, we have evaluated the corresponding fluxes as follows. In order to gain a first estimate we ignore the possibility of a nuclear crust which might shield the CFL phase. For large opacities, as implied by the results found above, the photon flux can be obtained from a convolution of the emissivity and mean free path, integrated over the photon energies. The neutrino flux, for simplicity, has been estimated by multiplying the emissivities and mean free paths as given in the first entry of Ref. [10], which amounts to the assumption that the neutrinos are thermalized when leaving the star.<sup>10</sup> To facilitate a direct comparison with the findings of Ref. [10], we have employed their values for the gap and the quark chemical potential,  $\Delta_0 = 100$  MeV and  $\mu_q = 400$  MeV, respectively. The results are displayed in Fig. 5, indicating that, despite of the extremely small mean free path of the photons, their emitted energy flux exceeds that of neutrinos by one to three orders of magnitude over a wide temperature range.<sup>11</sup>

Note that the photon flux approximately corresponds to that of a black-body emitter. This complies with the general expectation that, for very small photon mean free path, emission and absorption processes are close to equilibrium and reflect the surface temperature of the star.

## 4 Early Thermal Evolution

In this Section, we present a rough estimate of the early thermal evolution of a hypothetical CFL star. The thermal properties of CFL matter are expected to be dominated by the massless Goldstone boson  $\phi$ , which results from the breaking of the baryon number symmetry  $U(1)_B$ . The corresponding specific heat has been given in Ref. [9],

$$c_{v,\phi} = \frac{2\sqrt{3}\pi^2}{5} T^3 = 7.8 \times 10^{16} T_{\text{MeV}}^3 \text{ erg cm}^{-3} \text{ K}^{-1}. \quad (22)$$

The thermal conductivity in a CFL phase has been estimated in Ref. [30], where the contribution from the massless Goldstone boson was found to be

$$\kappa_\phi = 1.2 \times 10^{27} T_{\text{MeV}}^3 \lambda_{\text{cm}} \text{ erg cm}^{-1} \text{ s}^{-1} \text{ K}^{-1}, \quad (23)$$

with  $\lambda_{\text{cm}}$  being the mean free path of the Goldstone bosons in cm. The dominant process for the *mfp* is the decay of Goldstone bosons into pairs of quark quasiparticles. Assuming

---

<sup>10</sup>This is a good approximation for temperatures above a few MeV [10].

<sup>11</sup>Here we are implicitly assuming that photons and neutrinos are emitted at the same temperature. This does not hold, however, once a significant temperature gradient has established at the surface. In that case, neutrinos will be predominantly emitted from hotter regions in the interior, due to their larger mean free path.

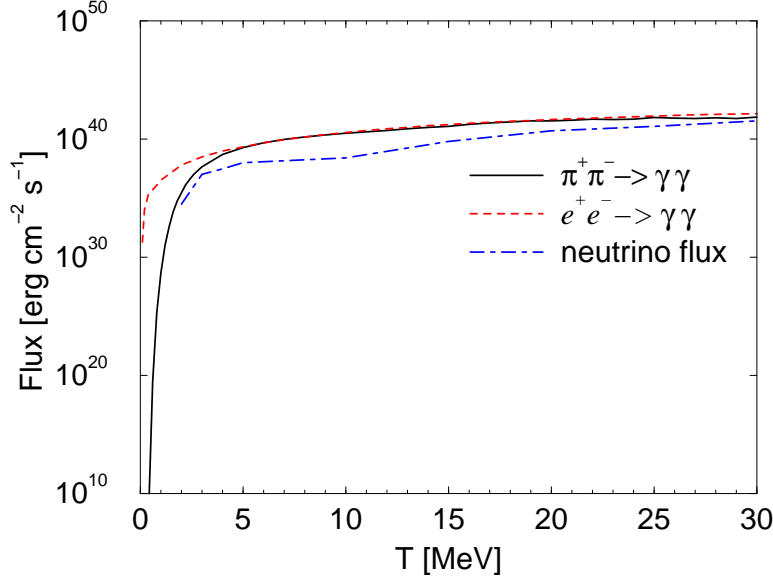


Figure 5: Comparison of photon and neutrino fluxes, with the parameter choice of Ref. [10],  $\Delta_0 = 100$  MeV and  $\mu_q = 400$  MeV.

thermalized Goldstone modes, the mean free path reads [30]

$$\lambda_{\phi \rightarrow qq}(T) \simeq \frac{4(21 - 8 \ln 2)}{15\sqrt{2}\pi T} \exp\left(\sqrt{\frac{3}{2}} \frac{\Delta}{T}\right). \quad (24)$$

Note that  $\lambda$  becomes large, *i.e.* greater than about 1 km, only for temperatures below 5 MeV.

Since, at large  $T$ , the thermal conductivity is extremely small, we may estimate the cooling time of the CFL surface in the very early stage by neglecting the heat transport in the interior of the star. We thus use the thermal energy,  $U_{\text{th,shell}}$ , stored in a shell with a thickness given by the photon mean free path,  $\Delta R \simeq \lambda_\gamma$ , to write the luminosity as

$$\frac{dU_{\text{th,shell}}}{dt} = -L_\gamma. \quad (25)$$

$U_{\text{th,shell}}$  is readily obtained by integrating the heat capacity over temperature and multiplying with the volume of the surface shell,

$$U_{\text{th,shell}} = 4\pi R^2 \lambda_\gamma \int_0^T c_{v,\phi}(T') dT'. \quad (26)$$

Using the black-body luminosity,  $L_\gamma = 4\pi R^2 \sigma T^4$ , together with Eq. (26) in expression (25), and setting the radius of the star to  $R = 10$  km, we find that the cooling time  $\Delta t$  of the shell is of the order

$$\Delta t \sim 10^{-16} \text{ s} \ln \frac{T_i}{T_f}, \quad (27)$$

with  $T_i$  being the initial and  $T_f$  the final temperature. This cooling time scale is extremely short, and is to be compared with the diffusion time of the massless Goldstone bosons, corresponding to the thickness  $\Delta R$  of the shell. The latter time scale might be assessed by the simple relation (see, *e.g.*, Ref. [12])

$$t_D = \left( \frac{\lambda_\gamma}{\lambda_\phi} \right)^2 t_{\text{int}}, \quad (28)$$

where  $t_{\text{int}} \simeq 10^{-20}$  s is the typical interaction time of the massless Goldstone bosons (estimated from their decay  $\phi \rightarrow qq$ ) at  $T \sim 30$  MeV. With  $\lambda_\phi(T = 30 \text{ MeV}) \sim 10^{-10}$  cm we find  $t_D \sim 10^{-14}$  s, which is much longer than the cooling time  $\Delta t$ . The large difference in these time scales justifies the neglect of the heat transport in the early stages of the cooling.

## 5 Summary and Conclusions

The main objective of this work has been an order of magnitude assessment of photon emission rates and mean free paths in a CFL phase of high-density quark matter. Our approach is based on a low-energy effective theory that describes the prevailing degrees of freedom at large densities and moderate temperatures,  $T \sim \mathcal{O}(10 \text{ MeV})$ . These are generalized Goldstone bosons that appear due to breaking of chiral and baryon number symmetries. We have followed the hidden local symmetry approach to introduce vector-meson excitations as well as the electromagnetic field in our analysis. The assumption of the KSRF relation in medium enabled us to relate the vector-meson self-interaction strength  $\tilde{g}$  and two-pion coupling  $g_{\rho\pi\pi}$  to the characteristic scales of the CFL phase, *i.e.*, the gap  $\Delta$  and the quark chemical potential  $\mu_q$ , according to  $g_{\rho\pi\pi} = \tilde{g} \simeq \sqrt{2} \Delta / f_\pi$ , where  $f_\pi \simeq 0.21 \mu_q$ . In the presence of in-medium modified pion dispersion relations, electromagnetic gauge invariance could be maintained by requiring both the  $\rho$ - $\gamma$  vertex as well as the rho propagator (with mass  $m_\rho \simeq 2\Delta$ ) in its vacuum form (which emerged as a consequence of neglecting the distinction between temporal and spatial components of the rho mass).

The resulting photon production and scattering amplitudes to lowest order have been convoluted over available phase space in CFL matter using standard kinetic theory expressions. Our results suggest that photon emissivities might become very large, up to  $\mathcal{O}(10^{53} \text{ erg cm}^{-3} \text{ s}^{-1})$  at the highest temperatures expected to occur during (or immediately following) a supernova explosion,  $T \simeq 30 \text{ MeV}$  [12]. Over a large range of CSC gap values,  $\Delta_0 = 50 - 150 \text{ MeV}$ , we find that at temperatures below  $\sim 5 \text{ MeV}$  the dominant process is  $e^+e^- \rightarrow \gamma\gamma$ , whereas for larger  $T$  electromagnetic pion annihilation,  $\pi^+\pi^- \rightarrow \gamma\gamma$ , is most important. Processes involving strongly interacting rho mesons could also play a major role. The temperature where the strong processes begin to outshine electromagnetic ones could not be accurately determined (although it might be well below 30 MeV), mostly due to uncertainties in the vector-meson mass spectrum. An interesting feature of the CFL phase is the appearance of the novel processes  $\pi^+\pi^- \leftrightarrow \gamma$ , which are triggered by the in-medium pion dispersion relation due to the breaking of Lorentz invariance.

We furthermore have found that the photon mean free path is extremely small over a wide range of temperatures. In particular, it is far below the typical radius of a compact star as long as the temperature is above about a few tens of keV. With a gap value of 50 (150) MeV,

the processes providing the largest opacity for  $T$  up to 5 (15) MeV are Compton scattering off thermal electrons and positrons,  $\gamma e^\pm \rightarrow \gamma e^\pm$ , as well as photon annihilation,  $\gamma\gamma \rightarrow e^+e^-$ , in agreement with previous calculations in a low-temperature approximation [31]. At larger  $T$ , Compton scattering off pions and photon annihilation into pion pairs are dominant.

The comparison with analogous calculations of neutrino properties in CFL matter [10] revealed that the photon emissivity is much larger than the neutrino one, whereas the mean free path is substantially shorter. A schematic estimate of the photon flux from a hypothetical CFL star with uniform temperature profile indicates that the photon flux could even exceed the volume-driven neutrino flux (temperature gradients will favor, however, the latter).

We have also presented an order of magnitude analysis of the cooling time of the outermost surface layers of a (hypothetical) CFL star, in the very early stages of its evolution. Since, at the highest temperatures considered here, the thermal conductivity of CFL matter is very small, one may neglect heat transport in the interior of the star. The thus found cooling time is of the order  $10^{-16}$  s. This is to be compared with the diffusion time of a massless Goldstone boson,  $t_D \sim 10^{-14}$  s, corresponding to the distance given by the photon mean free path at large temperature. These widely different time scales suggests that heat transport does not play a significant role in the very early cooling era.

Let us finally comment on a few aspects of our work that have not been adequately treated and should be addressed in future analyses:

(i) In our calculation of the emission rates and mean free paths we have restricted ourselves to the  $SU(2)$ -flavor case, *i.e.*, did not include contributions from strangeness-carrying mesons in the pseudoscalar and vector octet. The analysis of Ref. [18] showed that, while the  $K^-$  is slightly heavier than the pion, the  $K^+$  is considerably lighter. Since the sum of the kaon masses is less than the sum of the pion masses, one can expect that the emission rates from  $K^+K^-$  annihilation into photons will exceed the emission rates resulting from  $\pi^+\pi^-$  annihilation. Likewise, the kaon induced mean free path is expected to be smaller than the one induced by pions. Following our arguments of Sect. 3.4 we can assume, however, that the overall result for the flux will remain unchanged, being limited by black-body emission. At moderate densities, where the pion decay constant is of the order of the gap, one can also expect solitonic excitations in the baryon sector [25] to become relevant.

(ii) Our discussion of the cooling behavior of a compact star featuring CFL matter was limited to the very early stages of the thermal evolution, and we have furthermore made the simplifying assumption that the star accommodates a CFL phase which extends all the way up to the surface. We will postpone the investigation of the long-term cooling, including heat transport and more realistic scenarios in which the CFL phase is covered with a nuclear crust, to a future publication [32].

**Acknowledgements.** We would like to thank Emma Olsson, Chris Pethick, Robert Pirsarski, Igor Shovkovy, Kim Splittorff and Dmitri Voskresensky for interesting discussions. We are especially indebted to Francesco Sannino for his continuous encouragement throughout the work. C.V. wishes to thank Deirdre Black and Sanjay Reddy for many enlightening conversations, and the Theory Group at Jefferson Lab for their kind hospitality during his visit, where parts of this work have been done. He also thanks Igor Musatov for providing his program FeynmanGraph. This work is partially funded by the European Commission IHP program under contract HPRN-CT-2000-00130. The research of R. O. is supported by grants from the



Natural Science and Engineering Council of Canada (NSERC).

## A Appendix

### A.1 In medium Feynman rules

The Feynman rules follow from the effective Lagrangian discussed in Sect. 2 in a straightforward fashion. From the kinetic term in Eq. (1) we obtain the pion propagator,

$$i D_\pi = \frac{i}{p_0^2 - v_\pi^2 \mathbf{p}^2 - m_\pi^2 + i\epsilon} . \quad (29)$$

The vertex factors derive from the interaction part (14). For the  $\pi^+(p)\rho^0 \rightarrow \pi^+(p')$  vertex we find

$$i g_{\rho\pi\pi} (\tilde{p} + \tilde{p}')_\mu , \quad (30)$$

where  $\tilde{p} = (p_0, v_\pi^2 \mathbf{p})$ . The  $\pi^+\pi^-\rho^0\gamma$  contact vertex reads

$$2 i e g_{\rho\pi\pi} \tilde{g}_{\mu\nu} , \quad (31)$$

and for  $\pi^\pm\pi^0\rho^\pm\gamma$  we have

$$- i e g_{\rho\pi\pi} \tilde{g}_{\mu\nu} , \quad (32)$$

with  $\tilde{g}_{\mu\nu} = \text{diag}(1, -v_\pi^2, -v_\pi^2, -v_\pi^2)$ . The  $\pi^+\pi^-\gamma\gamma$  contact term is

$$- 2 i e^2 \tilde{g}_{\mu\nu} . \quad (33)$$

For the  $\rho^0$ - $\gamma$  coupling we obtain

$$- i \frac{e m_V^2}{\tilde{g}} g_{\mu\nu} . \quad (34)$$

Finally, the triple-rho vertex is given by

$$i g_{\rho\pi\pi} [g_{\mu\nu} (p - p')_\lambda + g_{\nu\lambda} (p' - q)_\mu + g_{\lambda\mu} (q - p)_\nu] , \quad (35)$$

where all momenta are flowing *into* the vertex.

### A.2 Process amplitudes

The process amplitudes for  $\pi^+(p_1)\pi^-(p_2) \rightarrow \gamma(q_1)\gamma(q_2)$  read

$$\mathcal{M}_{(1)}^{\mu\nu} = e^2 \frac{(2\tilde{p}_1 - \tilde{q}_1)^\mu (2\tilde{p}_2 - \tilde{q}_2)^\nu}{(E_1 - q_1)^2 - v_\pi^2 (\mathbf{p}_1 - \mathbf{q}_1)^2 - m_\pi^2} , \quad (36)$$

$$\mathcal{M}_{(2)}^{\mu\nu} = e^2 \frac{(2\tilde{p}_2 - \tilde{q}_1)^\mu (2\tilde{p}_1 - \tilde{q}_2)^\nu}{(E_2 - q_1)^2 - v_\pi^2 (\mathbf{p}_2 - \mathbf{q}_1)^2 - m_\pi^2} , \quad (37)$$

$$\mathcal{M}_{(3)}^{\mu\nu} = 2 e^2 \tilde{g}^{\mu\nu} . \quad (38)$$

By using crossing relations we immediately obtain the amplitudes for Compton scattering,  $\gamma \pi^\pm \rightarrow \gamma \pi^\pm$ , and  $\gamma \gamma \rightarrow \pi^+ \pi^-$ , relevant for the calculation of the photon mean free path.

The amplitudes for  $\pi^+(p_1) \pi^-(p_2) \rightarrow \rho^0(p_3) \gamma(q)$  are

$$\mathcal{M}_{(1)}^{\mu\nu} = e g_{\rho\pi\pi} \frac{(2\tilde{p}_1 - \tilde{q})^\mu (2\tilde{p}_2 - \tilde{p}_3)^\nu}{(E_1 - q)^2 - v_\pi^2 (\mathbf{p}_1 - \mathbf{q})^2 - m_\pi^2}, \quad (39)$$

$$\mathcal{M}_{(2)}^{\mu\nu} = e g_{\rho\pi\pi} \frac{(2\tilde{p}_2 - \tilde{q})^\mu (2\tilde{p}_1 - \tilde{p}_3)^\nu}{(E_2 - q)^2 - v_\pi^2 (\mathbf{p}_2 - \mathbf{q})^2 - m_\pi^2}, \quad (40)$$

$$\mathcal{M}_{(3)}^{\mu\nu} = 2e g_{\rho\pi\pi} \tilde{g}^{\mu\nu}, \quad (41)$$

where the indices  $\mu$  and  $\nu$  refer to the photon and rho meson polarisation, respectively. The amplitudes for  $\pi^\pm \rho^0 \rightarrow \pi^\pm \gamma$  and  $\rho^0 \rightarrow \pi^+ \pi^- \gamma$  directly follow from the above expressions through crossing.

For the processes  $\pi^\pm(p_1) \pi^0(p_2) \rightarrow \rho^\pm(p_3) \gamma(q)$  we find

$$\mathcal{M}_{(1)}^{\mu\nu} = -e g_{\rho\pi\pi} \frac{(2\tilde{p}_1 - \tilde{q})^\mu (2\tilde{p}_2 - \tilde{p}_3)^\nu}{(E_1 - q)^2 - v_\pi^2 (\mathbf{p}_1 - \mathbf{q})^2 - m_\pi^2}, \quad (42)$$

$$\mathcal{M}_{(2)}^{\mu\nu} = e g_{\rho\pi\pi} \frac{(2p_3 + q)^\mu (\tilde{p}_1 - \tilde{p}_2)^\nu - (\tilde{p}_1 - \tilde{p}_2)^\mu (2q + p_3)^\nu + g^{\mu\nu} (\tilde{p}_1 - \tilde{p}_2) \cdot (q - p_3)}{(p_3 + q)^2 - m_V^2}, \quad (43)$$

$$\mathcal{M}_{(3)}^{\mu\nu} = -e g_{\rho\pi\pi} \tilde{g}^{\mu\nu}. \quad (44)$$

The amplitudes for  $\pi^\pm \rho^\mp \rightarrow \pi^0 \gamma$ ,  $\pi^0 \rho^\pm \rightarrow \pi^\pm \gamma$  and  $\rho^\pm \rightarrow \pi^\pm \pi^0 \gamma$  can again be obtained by crossing.

### A.3 Pion width in a dense medium

The width of the pion, generated by its interaction with surrounding medium pions, is defined by  $\text{Im } \Sigma_\pi = -m_\pi \Gamma_\pi$ . The pion self-energy can be obtained from the standard expression (see, *e.g.*, Ref. [33])

$$\Sigma_\pi(k_0, \mathbf{k}) = \int \frac{d^3 p}{(2\pi)^3 2p_0} f^\pi(p_0, T) \mathcal{M}^{\pi\pi \rightarrow \pi\pi}, \quad (45)$$

where  $f^\pi$  is the Bose-Einstein distribution and  $\mathcal{M}^{\pi\pi \rightarrow \pi\pi}$  the forward-scattering amplitude of pions that scatter via ( $s$ -channel) rho-meson exchange. Upon evaluating  $\mathcal{M}$  in the center-of-mass (cms) frame, Eq. (45) takes the form

$$\Sigma_\pi(k_0, \mathbf{k}) = -\frac{2g_{\rho\pi\pi}^2}{(2\pi)^2} \int \frac{|\mathbf{p}| d|\mathbf{p}|}{p_0} f^\pi(p_0, T) \int_{s_{\min}}^{s_{\max}} \frac{ds}{|\mathbf{k}|} \frac{s/4 - m_\pi^2}{s - m_\rho^2 + i \text{Im } \Sigma_\rho}. \quad (46)$$

The integration limits for the integral over the squared cms energy  $s$  are given by  $s_{\min, \max} = 2m_\pi^2 + 2k_0 p_0 \pm 2|\mathbf{k}| |\mathbf{p}|$ , and

$$\text{Im } \Sigma_\rho = m_\rho \Gamma_\rho = \frac{g_{\rho\pi\pi}^2}{6\pi} \frac{q^3}{\sqrt{s}}, \quad q^2 = \frac{s}{4} - m_\pi^2. \quad (47)$$

For simplicity, we here neglect effects of the in-medium pion dispersion relation.

# References

- [1] J.C. Collins and M.J. Perry, Phys. Rev. Lett. **34**, 1353 (1975).
- [2] B.C. Barrois, Nucl. Phys. B **129**, 390 (1977);  
S.C. Frautschi, in Proceedings of the Workshop on *Hadronic Matter at Extreme Energy Density*, Erice, Italy, Oct 13-21, 1978, edited by N. Cabbibo and L. Sertorio (Plenum, New York, 1978), p. 18.
- [3] M.G. Alford, K. Rajagopal and F. Wilczek, Phys. Lett. B **422**, 247 (1998) [hep-ph/9711395].
- [4] R. Rapp, T. Schäfer, E.V. Shuryak and M. Velkovsky, Phys. Rev. Lett. **81**, 53 (1998) [hep-ph/9711396].
- [5] R.D. Pisarski and D.H. Rischke, Phys. Rev. Lett. **83**, 37 (1999) [nucl-th/9811104].
- [6] D.T. Son, Phys. Rev. D **59**, 094019 (1999) [hep-ph/9812287].
- [7] M.G. Alford, K. Rajagopal and F. Wilczek, Nucl. Phys. B **537**, 443 (1999) [hep-ph/9804403].
- [8] T. Schäfer, hep-ph/0304281.
- [9] P. Jaikumar, M. Prakash and T. Schäfer, Phys. Rev. D **66**, 063003 (2002) [astro-ph/0203088].
- [10] S. Reddy, M. Sadzikowski and M. Tachibana, Nucl. Phys. A **714**, 337 (2003) [nucl-th/0203011]; Phys. Rev. D **68**, 053010 (2003) [nucl-th/0306015].
- [11] P. Jaikumar, R. Rapp and I. Zahed, Phys. Rev. C **65**, 055205 (2002) [hep-ph/0112308].
- [12] S. L. Shapiro and S.A. Teukolsky, Black Holes, White Dwarfs, and Neutron Stars: the physics of compact objects (Wiley-Interscience, 1983).
- [13] S. Turbide, R. Rapp and C. Gale, hep-ph/0308085.
- [14] D.K. Hong, M. Rho and I. Zahed, Phys. Lett. B **468**, 261 (1999) [hep-ph/9906551].
- [15] R. Casalbuoni and R. Gatto, Phys. Lett. B **464**, 111 (1999) [hep-ph/9908227].
- [16] D.T. Son and M.A. Stephanov, Phys. Rev. D **61**, 074012 (2000) [hep-ph/9910491] [Erratum-*ibid.* **62**, 059902 (2000), hep-ph/0004095].
- [17] P.F. Bedaque and T. Schäfer, Nucl. Phys. A **697**, 802 (2002) [hep-ph/0105150].
- [18] T. Schäfer, Phys. Rev. D **65**, 074006 (2002) [hep-ph/0109052].
- [19] M. Rho, E.V. Shuryak, A. Wirzba and I. Zahed, Nucl. Phys. A **676**, 273 (2000) [hep-ph/0001104].

- [20] M. Bando, T. Kugo, S. Uehara, K. Yamawaki and T. Yanagida, Phys. Rev. Lett. **54**, 1215 (1985).
- [21] M. Bando, T. Kugo and K. Yamawaki, Phys. Rept. **164**, 217 (1988).
- [22] R.D. Pisarski and M. Tytgat, Phys. Rev. D **54**, 2989 (1996) [hep-ph/9604404].
- [23] R. Casalbuoni, Z. Duan and F. Sannino, Phys. Rev. D **63**, 114026 (2001) [hep-ph/0011394].
- [24] K. Kawarabayashi and M. Suzuki, Phys. Rev. Lett. **16**, 255 (1966);  
Riazuddin and Fayyazuddin, Phys. Rev. **147**, 1071 (1966).
- [25] A.D. Jackson and F. Sannino, hep-ph/0308182.
- [26] C. Manuel and M.H.G. Tytgat, Phys. Lett. B **501**, 200 (2001) [hep-ph/0010274].
- [27] M. Harada and K. Yamawaki, Phys. Rev. Lett. **87**, 152001 (2001) [hep-ph/0105335].
- [28] J. Kapusta, P. Lichard and D. Seibert, Phys. Rev. D **44** (1991) 2774  
[Erratum-*ibid.* D **47** (1993) 4171].
- [29] C. Song, Phys. Rev. C **47**, 2861 (1993).
- [30] I.A. Shovkovy and P.J. Ellis, Phys. Rev. C **66**, 015802 (2002) [hep-ph/0204132].
- [31] I.A. Shovkovy and P.J. Ellis, Phys. Rev. C **67**, 048801 (2003) [hep-ph/0211049].
- [32] R. Ouyed, R. Rapp and C. Vogt, in preparation.
- [33] R. Rapp and J. Wambach, Phys. Lett. B **351**, 50 (1995) [nucl-th/9502023].